# Stability of ecosystems under oscillatory driving with frequency modulation

Subhendu Bhandary,[1] Tanmoy Banerjee,[2,*] and Partha Sharathi Dutta[1,†]

[1]*Department of Mathematics, Indian Institute of Technology Ropar, Rupnagar 140 001, Punjab, India*

[2]*Chaos and Complex Systems Research Laboratory, Department of Physics, University of Burdwan, Burdwan 713 104, West Bengal, India*

(Received 9 January 2023; accepted 10 July 2023; published 2 August 2023)

Consumer-resource cycles are widespread in ecosystems, and seasonal forcing is known to influence them profoundly. Typically, seasonal forcing perturbs an ecosystem with time-varying frequency; however, previous studies have explored the dynamics of such systems under oscillatory forcing with constant frequency. Studies of the effect of time-varying frequency on ecosystem stability are lacking. Here we investigate isolated and network models of a cyclic consumer-resource ecosystem with oscillatory driving subjected to frequency modulation. We show that frequency modulation can induce stability in the system in the form of stable synchronized solutions, depending on intrinsic model parameters and extrinsic modulation strength. The stability of synchronous solutions is determined by calculating the maximal Lyapunov exponent, which determines that the fraction of stable synchronous solution increases with an increase in the modulation strength. We also uncover intermittent synchronization when synchronous dynamics are intermingled with episodes of asynchronous dynamics. Using the phase-reduction method for the network model, we reduce the system into a phase equation that clearly distinguishes synchronous, intermittently synchronous, and asynchronous solutions. While investigating the role of network topology, we find that variation in rewiring probability has a negligible effect on the stability of synchronous solutions. This study deepens our understanding of ecosystems under seasonal perturbations.

DOI: 10.1103/PhysRevE.108.024301

## I. INTRODUCTION

Oscillations in ecological communities are omnipresent, often characterized by peaks and valleys of species abundance [1,2]. The oscillating species abundance can show a plethora of nonequilibrium dynamics, including periodic, quasiperiodic, and chaotic motions over time [3–5]. The prevalence of oscillatory species dynamics is of significant interest, as their generation and persistence can support biodiversity maintenance [6,7]. Theoretical and empirical studies have shown that there are primarily two reasons for these oscillations: One reason is due to the interaction complexities among species in a community [3,8] and the other reason is due to the external driving in the form of regular seasonal forcing [5,9]. While previous studies have argued that oscillations in species abundance can be short lived without external driving, a recent study by Blasius *et al.* [10] has shown long persistence of self-sustained prey-predator cycles by employing a combination of laboratory experiments and mathematical analysis. Nevertheless, the effects of regular seasonal forcing on population cycles have been extensively studied [2,5,9]. In contrast, how perturbation or variation in seasonality can affect cyclic dynamics in species abundance is yet to be understood.

Perturbations in seasonal cycles are generally attributed to year-to-year variations in weather conditions. Moreover, many species span large geographical areas where the characteristic features of seasonal fluctuations, e.g., amplitude and frequency, can vary significantly [11]. Taylor *et al.* [12] have studied how variation in seasonality (in the form of breeding season length) affects cycles in a prey-predator population by introducing an exponent to the sinusoidal forcing term. Further, they have shown that variation in the forcing exponent can result in various bifurcations, including saddle-node, period-doubling, and Neimark-Sacker bifurcations [12]. Nonlinear systems are also known to respond differently with variation in forcing frequencies [13]. The effect of perturbations on the driving frequency (i.e., frequency modulation) of a phase oscillator and the van der Pol oscillator have been studied recently [14]. It has been shown that the stability region (in terms of the size of Arnold's tongue) of the system increases with an increase in the strength of frequency modulation and that is determined by negative values of the maximal Lyapunov exponent (MLE). Similar results also hold for a network of identical phase oscillators [15]. However, study of the interaction between endogenous population dynamics (e.g., nonlinear prey-predator interactions) and seasonal forcing with perturbed or time-varying frequency is lacking. Owing to current environmental changes [12], an inclusive theory for nonlinear population models, forced with perturbed seasonal cycles, is therefore necessary.

For a self-sustained periodic oscillator, the phase on a limit cycle is free; however, the phase on a periodic cycle of an externally forced system is related to the phase of the force. The key effect is phase locking and frequency entrainment of the oscillation to that of the force, resulting in synchronization between them [16,17]. Synchronization in nonlinear systems can also occur by noisy forcing [18,19]. The driven

*tbanerjee@phys.buruniv.ac.in

†Corresponding author: parthasharathi@iitrpr.ac.in

 

(response) system "forgets" its dynamics and initial condition and follows that of noisy forcing. Here we do not consider a population dynamics model with noisy forcing; instead, we perturb the natural forcing frequency by a time-dependent function. This translates a periodic driving force into a driving force with time-varying frequency or a frequency that experiences deterministic perturbation. Synchronization in such systems driven with an external oscillatory forcing with time-varying frequency has been studied by considering replicate systems with random initial conditions. It has been shown that for a constant driving frequency, the replicate systems do not forget their initial phase with variations in intrinsic system parameters; however, for a time-varying frequency perturbation, they may forget their initial phase and exhibit synchronous dynamics or synchronous dynamics interspersed with asynchronous dynamics. Once the system has attained a synchronous solution, its stability against perturbation can be determined by evaluating the MLE. A negative MLE signifies a stable synchronous solution [19]. These results have important implications in ecosystem dynamics, as spatial synchronization in species abundance is strongly connected with biodiversity maintenance [6,20].

Recently, the phenomenon of intermittent synchronization, i.e., when synchronous dynamics are interspersed with asynchronous dynamics, has attracted attention in the studies of complex population dynamics [21,22]. For a spatially coupled consumer-resource model, it has been shown that local species properties and dispersal strength can determine the occurrence of intermittent synchronization [21]. Intermittent synchronization is also observed in systems with time-varying coupling functions [23]. Fan *et al.* [22] have shown intermittent cluster synchronization in a spatial ecological network where the local dynamics is chaotic. None of these studies have considered forced models with frequency modulation. Suppose an oscillatory system that shows asynchronous dynamics without any frequency modulation can exhibit intermittent synchronization in the presence of frequency modulation. In that case, the intermittent synchronous dynamics can be considered as transient, and in ecosystems, the importance of transient dynamics has been increasingly recognized [24].

To explore the role of frequency modulation in determining the dynamics of cyclic ecosystems, we consider the Rosenzweig-MacArthur [25] model of consumer-resource interaction. The growth rate of a dimensionless model is then perturbed with a sinusoidal forcing whose frequency changes depending upon a time-dependent function. With variations in model parameters, the forced system exhibits a variety of collective dynamics that includes synchronous, intermittent synchronous, or asynchronous dynamics; however, in the absence of forcing, these dynamics were absent. Similar results have also been obtained for a spatial network model. We reduce the network model to a phase equation by applying the phase-reduction method, which clearly distinguishes synchronous, intermittent, or asynchronous dynamics between nodes in terms of phase differences. The stability of the observed collective dynamics has also been determined by calculating the MLE. Our results are robust as they occur in a large region of system parameter space and network topology. Notably, intermittent synchronization has never been reported in a forced ecological system and enriches our understating of temporally perturbed population dynamics.

## II. MATHEMATICAL MODELS

### A. Consumer-resource model with frequency modulation

Here we consider a consumer-resource model following Rosenzweig and MacArthur [25], consisting of a resource density $X$ and a consumer density $Y$. The two-species model is given as

$$\frac{dX}{d\tau} = rX\left(1-\frac{X}{K}\right) - \frac{aXY}{b+X}, \tag{1a}$$

$$\frac{dY}{d\tau} = \frac{caXY}{b+X} - mY, \tag{1b}$$

where $r$ denotes the intrinsic growth rate, $K$ is the carrying capacity of the resource $X$, $a$ represents the predation rate, $b$ is the value of $X$ where predation is at half maximum, $c$ denotes the efficiency of $Y$ through predation, and $m$ is its natural mortality rate.

In earlier studies, the intrinsic growth rate of resource $r$ was considered as either constant or varying periodically, having a constant frequency to discern consumer-resource dynamics under periodic forcing [13]. Here, to study consumer-resource dynamics in a fluctuating environment, we incorporate perturbation in the resource growth rate $r$ of Eq. (1) with time-varying frequency, mathematically modeled as an oscillator with time-varying frequency. We consider $r \to r[1+\eta\sin(\theta_0)]$, i.e., the resource growth rate is forced with strength $\eta$ ($\geqslant 0$) and phase $\theta_0$. The phase $\theta_0$ evolves in time as $\frac{d\theta_0}{dt} = w_0[1+\gamma g(w_f t)]$, where $g$ is a single-tone periodic function of the form $g(w_f t) = \sin(w_f t)$, $w_0$ is the nonmodulated frequency, and $\gamma$ and $w_f$ are the strength and frequency of the imposed modulation or perturbation on the natural driving frequency $w_0$, respectively. Note that when $\gamma = 0$, $\theta_0 = w_0 t$ and the system is periodically forced.

By the substitutions $x = \frac{X}{b}$, $y = \frac{aY}{rb}$, $t = \tau r$, $\alpha = b/K$, $\phi = \frac{ca}{r}$, and $\mu = \frac{m}{r}$ and incorporating the perturbation in $r$, Eq. (1) is transformed into the nondimensional model

$$\frac{dx}{dt} = [1+\eta\sin(\theta_0)]x(1-\alpha x) - \frac{xy}{1+x}, \tag{2a}$$

$$\frac{dy}{dt} = \frac{\phi xy}{1+x} - \mu y, \tag{2b}$$

with nonautonomous perturbation in the forcing frequency, following $\theta_0 = w_0[t - \frac{\gamma}{w_f}\cos(w_f t)]$. The dimensionless parameters $\alpha$, $\phi$, and $\mu$ represent the strengths of prey self-regulation, prey-to-predator conversion rate, and predator mortality rate, respectively [26], which determine the species' local dynamics. Unlike other well-studied seasonally forced population models [5,13,27], the model (2) does not have a periodic forcing as $\theta_0$ in Eq. (2a) varies with time. Such a variation in resource growth rate can be considered time-varying driving, which may arise due to irregular environmental changes. We consider parameter values of the uncoupled model of $\eta = 0.3$, $\alpha = 0.3$, $\phi = 2$, $\mu = 1$, $w_0 = 0.541$, and $w_f = 0.01$ throughout this paper unless mentioned otherwise.

### B. Spatial ecological network of consumer-resource interactions with frequency modulation

Next we study a spatial network of consumer-resource interactions, where the population dynamics in each patch or node is governed by Eq. (2). The species dynamics in the $i$th patch are modeled as

$$\frac{dx_i}{dt} = [1+\eta\sin(\theta_0)]x_i(1-\alpha x_i) - \frac{x_i y_i}{1+x_i} + \epsilon_1\sum_{j=1}^{N} A_{ij}(x_j - x_i), \tag{3a}$$

$$\frac{dy_i}{dt} = \frac{\phi x_i y_i}{1+x_i} - \mu y_i + \epsilon_2\sum_{j=1}^{N} A_{ij}(y_j - y_i), \tag{3b}$$

where $i = 1, 2, \ldots, N$ and $N$ denotes the total number of nodes. We assume identical dynamics in all the nodes, and species follow diffusive dispersal between the nodes [26]. Like the uncoupled model (2), here also the seasonal forcing frequency is modulated as $\theta_0 = w_0[t - \frac{\gamma}{w_f}\cos(w_f t)]$. The parameters $\epsilon_1$ and $\epsilon_2$ represent resource and consumer dispersal rates, respectively. For simplicity, we consider the parameters $\epsilon_1 = \epsilon_2 = \epsilon$. The interaction matrix $A$ determines the species' dispersal between nodes. An element $A_{ij}$ of $A$ is equal to 1 if nodes $i$ and $j$ are connected and 0 otherwise. The number of links in each node (the degree of each node) is represented by $k_i$, where $k_i = \sum_{j=1}^{N} A_{ij}$. Elements of the matrix $A$ can change depending on the connectivity patterns of species, which have been widely used to study the collective dynamics of coupled oscillators [26,28]. We consider that species dispersal follows the Watts-Strogatz network, which can form three types of interaction network structure depending upon the rewiring probability $p$: regular, small world, and random. For example, the network is regular if $p = 0$, totally random when $p = 1$, and small world for $0 < p < 1$. Without loss of generality, in all our simulations for a particular network, we choose a fixed value of the average degree $k$. We use the fourth-order Runge-Kutta method with adaptive step size for numerical simulation of the models.

## III. RESULTS

### A. Complex dynamics of the consumer-resource model with oscillatory driving

#### 1. Cyclic species abundance and sensitive dependence on initial phase

The driven consumer-resource model (2) can produce an array of interesting complex dynamics that includes quasiperiodicity, chaos, and synchronization via a common driving force. In the absence of any forcing or perturbation (i.e., $\eta = 0$), the model (2) has three equilibrium points: one coexistence equilibrium point at $(\frac{\mu}{\phi-\mu}, \frac{\phi(\phi-\mu-\alpha\mu)}{(\phi-\mu)^2})$, one resource only equilibrium point at $(\frac{1}{\alpha}, 0)$, and one trivial equilibrium point at (0,0). The coexistence equilibrium point changes its stability via a supercritical Hopf bifurcation at $\alpha = \frac{\phi-\mu}{\phi+\mu}$ and there exists a stable limit cycle when $\alpha < \frac{\phi-\mu}{\phi+\mu}$. Figure 1(a) presents the bifurcation diagram of (2) with variation in the parameter $\alpha$. For the chosen parameter values, the Hopf bifurcation occurs at $\alpha \approx 0.33$.

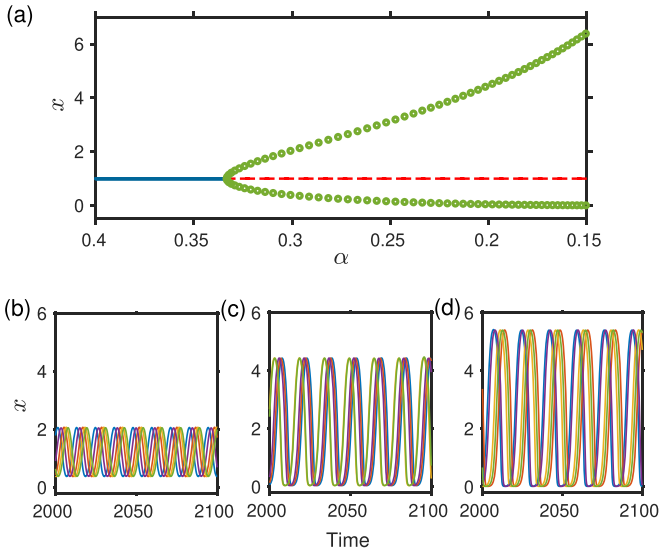


FIG. 1. Bifurcation diagram and time series of the population model (2) in the absence of external driving ($\eta = 0$). (a) Bifurcation diagram depicting the transition from a stable equilibrium point to a limit cycle with decreasing parameter $\alpha$. The solid curve before the bifurcation point represents a stable equilibrium point and circled curves after the bifurcation point present upper and lower amplitudes of the limit cycle. The dashed curve represents an unstable equilibrium point. Also plotted are five trajectories for randomly chosen initial conditions when (b) $\alpha = 0.3$, (c) $\alpha = 0.201$, and (d) $\alpha = 0.173$. The other parameters are $\phi = 2$ and $\mu = 1$.

Figures 1(b)–1(d) depict time series of (2) for different values of the parameter $\alpha$ when $\eta = 0$ (strength of seasonal perturbation). In each figure we present five trajectories simulated using five randomly chosen initial conditions. Note that, with a decrease in $\alpha$, the oscillation period increases and hence the oscillation frequency decreases. However, none of the trajectories forget their initial phase and all maintain a constant phase difference throughout time. In the presence of perturbation (nonzero values of $\eta$ and $\gamma$), the periodic oscillation can turn into quasiperiodic or chaotic oscillations and the system may experience phase-forgetting behavior [19].

#### 2. Synchronization by time-varying driving force

Synchronization between a driven (response) system and a driving system occurs when the driven system forgets its dynamics and follows the driver. Here we study the driven system's sensitivity to perturbation on the driving force, which appears in Eq. (2) for a nonzero value of $\gamma$ and via the function $g(w_f t)$. Following [14,19], in this case synchronization can be studied if we compare identical systems driven with the common perturbed external force but for different initial conditions. We integrate Eq. (2), considering $\gamma \neq 0$ for different initial conditions $(x_0, y_0)$ chosen randomly from $[0, 3] \times [0, 3]$, to find whether the trajectories synchronize or not upon the presence of frequency modulation. We find that the trajectories can exhibit synchrony, intermittent synchrony, or asynchrony [see Figs. 2(a)–2(c)] depending upon the choice of the strength of prey self-regulation $\alpha$. At $\alpha = 0.3$, all the trajectories of the replicate systems of (2) synchronize for

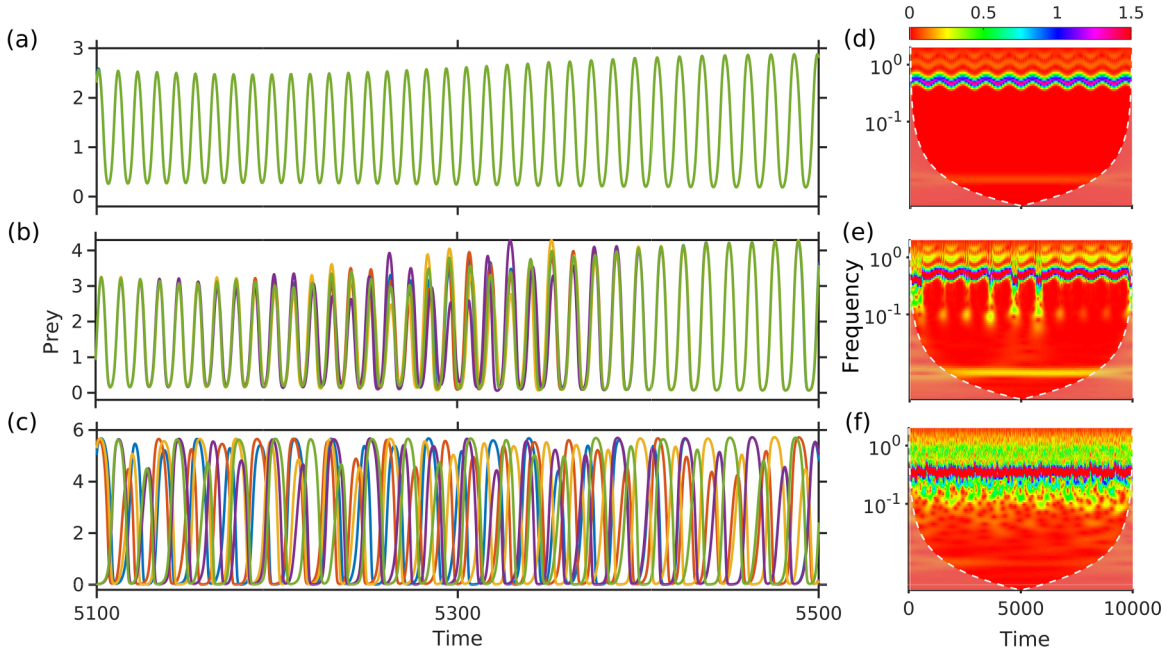


FIG. 2. Sensitivity to perturbation of the driving force $w_0$ on the stability of the driven system with variations in prey self-regulation $\alpha$. Five replicates of the model (2) have been simulated for randomly chosen initial conditions $(x_0, y_0) \in [0, 3] \times [0, 3]$. Three different dynamics occur with variations in $\alpha$: (a) For $\alpha = 0.3$ all solutions synchronize, (b) for $\alpha = 0.201$ solutions exhibit intermittent synchrony, and (c) for $\alpha = 0.173$ all solutions behave differently and asynchrony occurs. (d)–(f) Morlet wavelet transform of a trajectory in different dynamical regions. (d) Frequency entrainment and a stable phase are observed throughout the entire time, (e) frequency entrainment occurs periodically, resulting in intermittent synchronization, and (f) no frequency entrainment occurs. The other parameter values are $\phi = 2$, $\mu = 1$, $\eta = 0.3$, $\gamma = 0.1$, $w_0 = 0.541$, and $w_f = 0.01$.

different randomly chosen initial conditions though they are not directly coupled. Here synchronization between the driven replicate systems also corresponds to the stability of the driven system for internal perturbations [19]. This was not the case without perturbation (see Fig. 1). In fact, this can be attributed to phase-forgetting behavior resulting from the forcing with time-varying frequency. For $\alpha = 0.201$, the replicate systems undergo intermittent synchronization when events of synchronous species abundance are interspersed with events of asynchrony with variations in time. For $\alpha = 0.173$, complete asynchrony occurs, i.e., the replicate systems of (2) oscillate differently and do not synchronize. Therefore, one may also conclude that the driven system (2) is not stable upon the perturbation on the driving force when $\alpha = 0.173$.

With variations in $\alpha$, the difference in sensitivity to initial conditions is verified further using the time-frequency representation or wavelet transform of all the trajectories. Figure 2(d) represents complete synchrony between all the oscillators corresponding to Fig. 2(a). Similarly, the wavelet transforms in Figs. 2(e) and 2(f) represent intermittent synchrony and asynchrony corresponding to Figs. 2(b) and 2(c), respectively.

The dynamics of the driven system are synchronized if they are stable against the internal perturbation given in the driver's natural forcing frequency $w_0$. This can also be quantified by numerically calculating the MLE. A negative value of the MLE determines the occurrence of synchronization [19] and hence stability against the perturbations. Further, a non-negative value of the MLE determines either asynchrony or intermittent synchrony of the system. Figure 3 presents the MLE for the model (2) calculated for combinations of $\alpha$ and $\eta$ and different values of the strength of frequency modulation $\gamma$. Figure 3(a) depicts the case of no frequency modulation: It shows a broad region of unsynchronized solution (characterized by a positive MLE). However, we find that the stability region of the system broadens with an increase in $\gamma$ as the fraction of the negative MLE increases [see Figs. 3(b)–3(d)].

An explanation for the observed dynamics could be the frequency mismatch between the unforced system's frequency and the unperturbed forcing frequency $w_0$. As discussed and evident from Fig. 1, with a decrease in $\alpha$, the frequency of the unforced system decreases. Here a decrease in $\alpha$ leads to an increased frequency mismatch. Synchronization occurs when the frequency mismatch is approximately zero. At $\alpha = 0.3$, the system's frequency is almost the same as $w_0$, which leads to complete synchrony. At $\alpha = 0.173$, frequency mismatch is maximum and we observe complete asynchrony.

### B. Dynamics of spatial ecological network under frequency modulation

#### *1. Intermittent synchronization in spatial ecological networks*

Next we study the effect of frequency modulation on the synchronicity of the seasonally forced ecological network model (3). Here synchronization means spatial synchronization between nodes, not sensitivity to initial conditions, as shown in the preceding section. In the absence of any forcing ($\eta = 0$), we find that the network system exhibits asynchrony for weak dispersal strength ($\epsilon = 2^{-7}$) and variations in $\alpha$. However, the weakly coupled system exhibits interesting

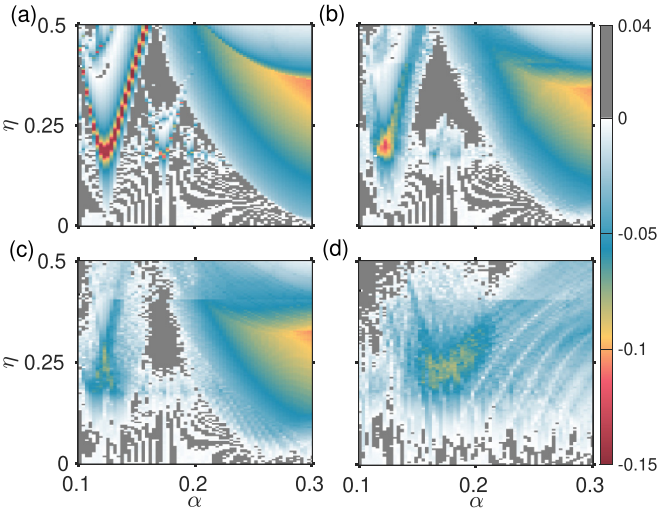


FIG. 3. Maximal Lyapunov exponent calculated numerically in the $(\alpha, \eta)$ parameter space for different values of $\gamma$. We have depicted the MLE, calculated for a longer time interval, and averaged over 50 initial conditions sampled randomly from $[0, 3] \times [0, 3]$. The MLE has been calculated for the following values of $\gamma$: (a) $\gamma = 0$ (no frequency modulation), (b) $\gamma = 0.05$, (c) $\gamma = 0.1$, and (d) $\gamma = 0.4$. The color bar represents the values of the MLE. With an increase in the modulation strength $\gamma$, the region of the stable synchronous solution increases as determined by negative values of the MLE. The other parameters are $\phi = 2$, $\mu = 1$, $w_0 = 0.541$, and $w_f = 0.01$.

spatial dynamics in the presence of frequency modulation ($\eta \neq 0$ and $\gamma \neq 0$). Figure 4 shows the spatial dynamics of the network model (3) with perturbation in the resource growth rate. As observed, the perturbed system undergoes synchronization, intermittent synchronization, and asynchronization dynamics for different values of $\alpha$. At $\alpha = 0.3$, we observe spatial synchronization [see Figs. 4(a) and 4(d)], and for $\alpha = 0.173$ the system exhibits asynchronization [see Figs. 4(c) and 4(f)] between spatially separated nodes. However, for $\alpha = 0.201$ we obtain intermittent synchronization as depicted in Figs. 4(b) and 4(e).

The degree of synchronous dynamics between nodes in a network can also be evaluated via the phase response curve (PRC) [29]. To calculate the PRC for the considered network model, one needs to convert the phase-amplitude oscillator equation into a phase equation by employing the phase-reduction method. We will discuss this in detail in the next section.

### 2. *Phase reduction of the forced network model*

The phase-reduction method [30] is a useful tool in explaining the evolution of phases in multidimensional systems, thereby giving a clearer picture of the stability of synchronous solutions. Thus far, its application in ecological networks has been limited [31,32]. Here, using the phase-reduction method, we derive analytical expressions for the type of phase lock in the network model (3) and the rate of convergence to the phase-locked state [33,34]. We begin by expressing the model (3) in a general form as

$$\frac{dX_i}{dt} = F(X_i) + \epsilon \sum_{j=1}^{N} A_{ij} C(X_j, X_i) + \eta I(X_i) p(t), \qquad (4)$$

where $X_i = [x_i, y_i]$, $F(X_i) = [F_1(X_i), F_2(X_i)]$, $I(X_i) = [x_i(1 - \alpha x_i), 0]$, and $p(t) = \sin\{w_0[t - \frac{\gamma}{w_f}\cos(w_f t)]\}$. The function $F(X_i)$ represents the unperturbed dynamics of the $i$th node, $C(X_i, X_j)$ denotes the effect of the $i$th node on the $j$th node, and $I(X_i)$ is the perturbation in the $i$th node. The $A_{ij}$ is an element of the interaction matrix $A$, which represents the interaction strength between the $i$th and $j$th nodes. The system $\frac{dX_i}{dt} = F(X_i)$ exhibits a stable limit cycle $S$ of period $T$. The limit cycle $S$ has its natural frequency $\omega = \frac{2\pi}{T}$ and an oscillator state on $S$ is denoted by $X_0(\theta)$. We denote by $\Theta(X)$ the phase function of $S$ and by $Z(\theta)$ the phase-sensitivity function

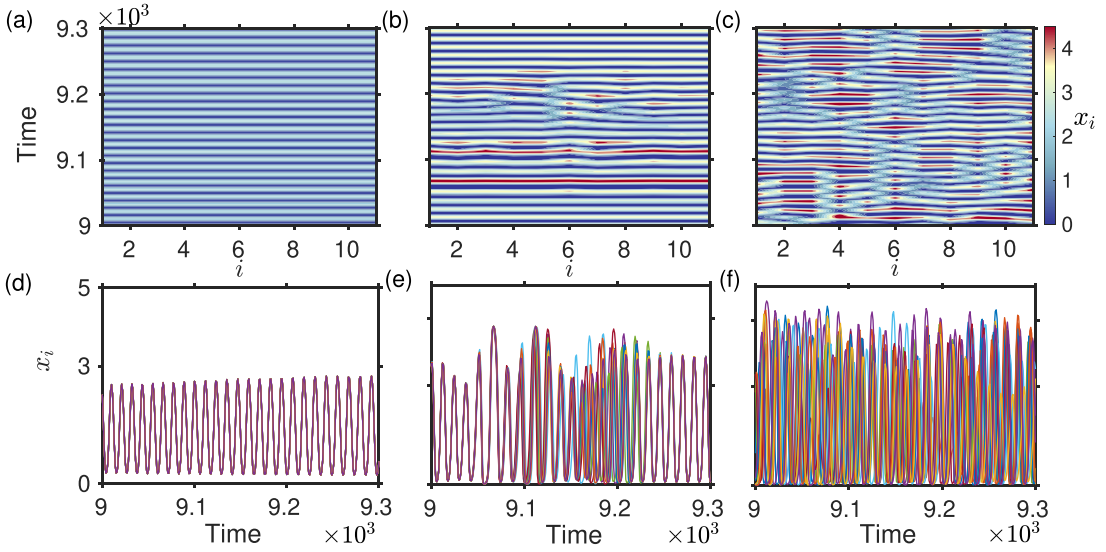


FIG. 4. Space-time and corresponding time series plots of the network model (3) for different values of $\alpha$: (a) and (d) synchronous species oscillations when $\alpha = 0.3$, (b) and (e) intermittent synchronous oscillations for $\alpha = 0.201$, and (c) and (f) asynchronous oscillations for $\alpha = 0.173$. The other parameter values are $\phi = 2$, $\mu = 1$, $\eta = 0.25$, $\gamma = 0.05$, $w_0 = 0.541$, $w_f = 0.01$, $\epsilon = 2^{-7}$, $k = 1$, $p = 0$, and $N = 11$.

of $S$. Consequently, the phase of the $i$th oscillator or node is written as $\theta_i(t) = \Theta(X_i(t))$. Further, we can approximate $X_i(t)$ as a function of $X_0(\theta_i(t))$ on $S$. The reduced approximate phase of the $i$th node is given by

$$\begin{aligned}\frac{d\theta_i}{dt} &= \frac{d}{dt}\Theta(X_i(t)) = \mathrm{grad}_{X_i}\Theta(X_i)|_{X_i=X_i(t)}\frac{dX_i}{dt}\\ &\approx \mathrm{grad}_{X_i}\Theta(X_i)|_{X_i=X_0[\theta_i(t)]}\\ &\quad\times\left(F(X_i)+\epsilon\sum_{j=1}^{N}A_{ij}C(X_j,X_i)+\eta I(X_i)p(t)\right)\\ &= w+\epsilon\sum_{j=1}^{N}A_{ij}\Gamma(\theta_j-\theta_i)+\eta Z(\theta_i)I(\theta_i)p(t),\end{aligned}$$

where the effect of coupling on a phase of each oscillator is determined as

$$\Gamma(\phi)=\frac{1}{2\pi}\int_0^{2\pi}Z(\phi+\xi)C(X_0(\phi+\xi),X_0(\xi))d\xi. \quad (5)$$

Here $\phi$ represents the phase difference between two oscillators. We have calculated the phase coupling function $\Gamma(\phi)$, which represents the effect of one oscillator on another oscillator over one period of the limit cycle oscillation. Here $Z(\theta_i) = \mathrm{grad}_{X_i}\Theta(X_i)|_{X_i=X_0(\theta_i(t))}$ represents the phase response curve which measures the effect of small perturbations on the phase dynamics. Advance (delay) of the phase is denoted by a positive (negative) value of the PRC induced by perturbations in the phase. We numerically computed the PRC using the adjoint equation considering one stable limit cycle. The PRC is evaluated by Malkin's approach [35,36] using the adjoint equation

$$w\frac{dZ(\theta_i)}{d\theta_i} = -J(\theta_i)^T Z(\theta_i), \quad (6)$$

with the normalization condition

$$Z(\theta_i)\frac{dX_0(\theta_i)}{d\theta_i} = w. \quad (7)$$

Thereafter, we numerically evaluate $Z(\theta)$ and $\Gamma(\phi)$, owing to the nonlinearity of the considered model. We calculate $\Gamma$ from Eq. (5) and $Z$ from Eqs. (6) and (7). Using the above calculated PRC value, we can convert our coupled system [Eq. (3)] into an $N$-dimensional phase equation and further study its phase dynamics. To determine a synchronous solution, we calculate the phase differences of all the coupled oscillators ($\phi_{1i} = \theta_1 - \theta_i$, $i = 2, 3, \ldots, N$) as shown by

$$\frac{d\phi_{1i}}{dt} = \frac{d\theta_1}{dt} - \frac{d\theta_i}{dt} = \epsilon\left(\sum_{j=1}^{N}A_{1j}\Gamma(\theta_j-\theta_1) - \sum_{j=1}^{N}A_{ij}\Gamma(\theta_j-\theta_i)\right) + \eta p(t)[Z(\theta_1)I(\theta_1) - Z(\theta_i)I(\theta_i)] = G(\phi_{1i}). \quad (8)$$

The differential equation (8) represents the evolution of phase differences over time. Here $G$ determines the stability of the phase-locked state and the rate of convergence of the synchronized state. A constant phase difference or a phase-locked state occurs when $G = 0$. The sign of $G$, negative or positive, determines if the steady states of the phase equation are stable or unstable, respectively. We are interested in studying the rate of convergence to the phase-locked states, i.e., synchrony or asynchrony for different parameter regimes. Actually, the rate of convergence to that state helps us understand synchrony in population abundances, which determines the rate of species persistence in shorter or longer timescales. Plotted in Fig. 5(a) is a phase portrait which shows the existence of a stable limit cycle in the system (3), and the corresponding time series for $x$ and $y$ are shown in Fig. 5(b). We have also calculated the PRC $Z(\theta_i)$ from the adjoint variational equations (6) and (7) and it is plotted in Fig. 5(c). The numerically calculated $G$ function, which represents the phase change rate between two nodes, is plotted in Fig. 5(d).

We have numerically obtained intermittent synchrony for frequency modulation in the system. After applying the phase-reduction method in (3), we can now clearly differentiate between synchrony, intermittent synchrony, and asynchrony by evaluating changes in the phase angle for the spatial ecological network model. For different $\alpha$, we calculate the phase difference $|\theta_i - \theta_1|$ of each reduced phase oscillator $\theta_i$ to the first oscillator $\theta_1$ [see Figs. 6(a)–6(c)]. In Fig. 6(a), for high $\alpha$ (=0.3), phase difference is zero beyond transient time, and

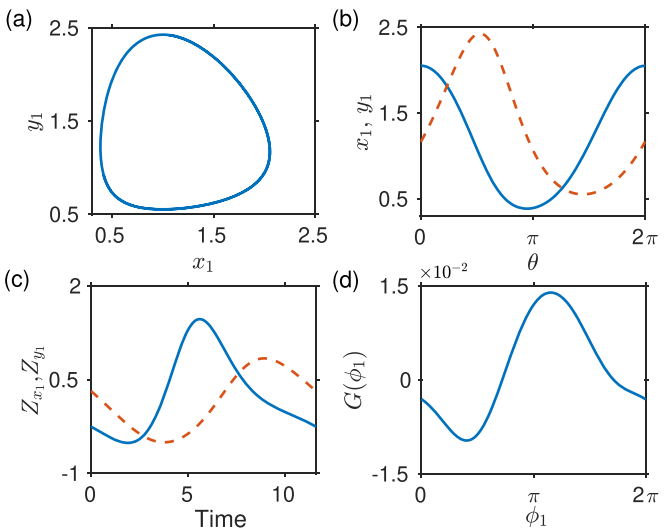


FIG. 5. (a) Phase portrait of a node depicting a limit cycle and (b) corresponding time series. The variable $x$ represents resource abundance shown by the blue solid curve and the variable $y$ denotes consumer abundance plotted by the red dashed)curve. (c) Phase response curve, which is the bounded solution $Z(t) = (Z_x(t), Z_y(t))$ of the adjoint variational equation (6) for one time period $T = 11.6$ and when $\eta = 0$. (d) Function $G(\phi)$ describes the phase change rate between two nodes. Here $G(\phi_{1i}) = 0$ signifies the phase-locked state. The other parameter values are $\phi = 2, \alpha = 0.3, \mu = 1, \eta = 0.25, \gamma = 0.1, w_0 = 0.541, w_f = 0.01, \epsilon = 2^{-7}, k = 1, p = 0$, and $N = 11$.

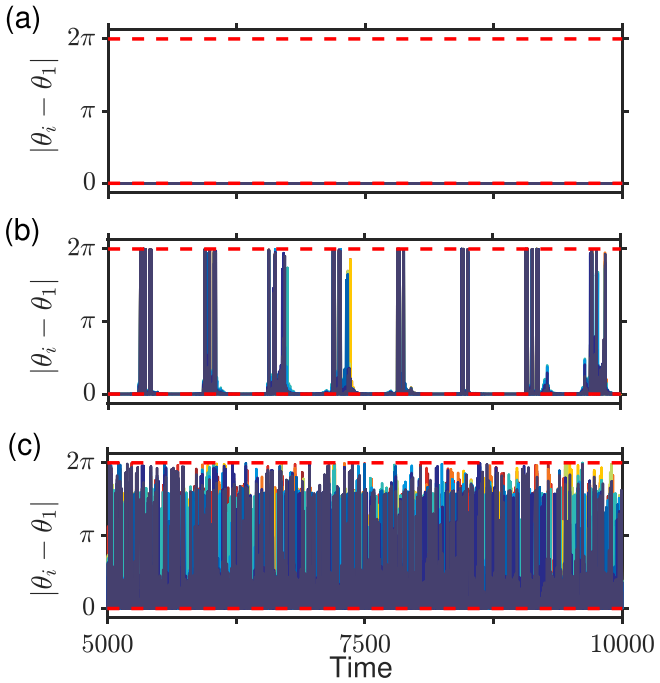


FIG. 6. Averaged phase difference calculated over 100 initial conditions for the network model in Eq. (8). The phase difference $|\phi_{1i}| = |\theta_i - \theta_1|$ of the first oscillator with other oscillators is shown for different values of prey self-regulation: (a) $\alpha = 0.3$, (b) $\alpha = 0.201$, and (c) $\alpha = 0.173$. The other parameter values are $\phi = 2$, $\mu = 1$, $\eta = 0.25$, $\gamma = 0.05$, $w_0 = 0.541$, $w_f = 0.01$, $\epsilon = 2^{-7}$, $k = 1$, $p = 0$, and $N = 11$.

phase synchronization between nodes occur. For an intermittent $\alpha$ (=0.201) value, the phase difference switches between zero and nonzero values, which represent intermittent synchronization [see Fig. 6(b). In Fig. 6(c) we observe that the phase difference is always nonzero and asynchronous dynamics occur when $\alpha = 0.173$. Further, for a fixed $\alpha$, inclusion of frequency modulation via a nonzero value of $\gamma$ can flip the asynchronous dynamics into synchronous dynamics [see Figs. 9(a)–9(d) in the Appendix].

#### 3. *Extent of synchronicity between nodes in the spatial network*

Though in the previous sections we have determined various synchronization patterns between the oscillating nodes with variations in system parameters, it is further possible to quantify how good the synchrony is via the synchronization order parameter $\rho$ [37]. We measure $\rho$, the extent of synchrony with variations in the coupling strength $\epsilon$, the strength of external forcing $\eta$, and species self-regulation $\alpha$ for different values of the strength of frequency modulation $\gamma$. The synchrony order parameter $\rho$ is defined as [37]

$$\rho = \sqrt{\left\langle \frac{\bar{z}(t)^2}{\frac{1}{N}\sum_{i=1}^{i=N} z_i(t)^2} \right\rangle}, \tag{9}$$

where $z_i(t)$ is the system's state at time $t$, $\bar{z}(t) = \frac{1}{N}\sum_{i=1}^{N} z_i(t)$, and $\langle \cdots \rangle$ denotes the average over a long time $T$. The order parameter value $\rho$ varies between 0 to 1. A value close to 0 indicates no synchronization and 1 indicates perfect synchronization. If $0 < \rho < 1$, partial synchronization will occur. For the model (3), at each fixed $\gamma$, $\rho$ is computed in the presence of frequency modulation.

In Figs. 7(a)–7(c), at different $\gamma$, the synchrony measure $\rho$ is shown for varying coupling strength $\epsilon$ and prey self-regulation $\alpha$. We find that for high values of $\alpha$, the network exhibits synchronization irrespective of the choice of $\epsilon$ and $\gamma$. Notably, higher values of $\gamma$ induce synchrony in the system at a lower value of $\alpha$ than lower values of $\gamma$ do. Therefore, higher-frequency modulation strength is capable of better synchronizing the system. Figures 7(d)–7(f) depict the synchrony measure with variations in $\epsilon$ and $\eta$, at different values of $\gamma$. We find that a higher value of $\gamma$ results in better synchronization in the network irrespective of the choice of $\epsilon$ and $\eta$. Overall, the synchrony order parameter $\rho$ determines that for high-frequency oscillations (higher-$\alpha$ value) high strength external forcing can be detrimental to species persistence as it induces a higher degree of synchrony in species abundance.

#### 4. *Effect of network structure on the stability of synchronous solution*

We also investigate the impact of network properties such as rewiring probability $p$ and average degree $k$ on synchronization stability by calculating the MLE with variations in $\alpha$ and $\eta$ when $N = 21$. In Figs. 8(a) and 8(b) we observe that the stability region of the synchronized solution does not change appreciably with $p$. The Lyapunov exponent is either zero or positive for low $\alpha$ and $\eta$, indicating an unstable synchronization manifold. However, the synchronization manifold is stable in regions of higher $\alpha$ and $\eta$ values as determined by a negative Lyapunov exponent. However, a larger average degree $k$ results in a broader synchronized zone: Figures 8(c) and 8(d) show that an increase in $k$ has a positive effect on the stability of the synchronization manifold.

## IV. CONCLUSION

Previous research on the dynamics of seasonally forced ecosystem models has mostly considered oscillatory forcing with a constant frequency. Thus, they have the limitation of capturing natural disturbances as, in reality, a seasonal forcing may not always maintain a constant frequency of oscillations. Owing to the present environmental changes, irregularity in seasonality is becoming more evident. Here, to bridge this gap, we studied the dynamics of a driven population model whose forcing frequency of the perturbation varies over time. We found that frequency modulation can result in intermittent synchronization, other than complete synchronization and asynchronization. The occurrence of intermittent synchronization in a driven ecological system can be attributed to transient dynamics. Transients are fundamentally crucial to ecosystems with implications for biodiversity maintenance and biological control [24]. We also evaluated the MLE, which measures the stability of the synchronized solution. Owing to the model nonlinearity and time dependence of the forcing frequency, unlike other studies [38], we did not obtain a clear Arnold tongue region (region of negative Lyapunov exponent) over the parameter space of the

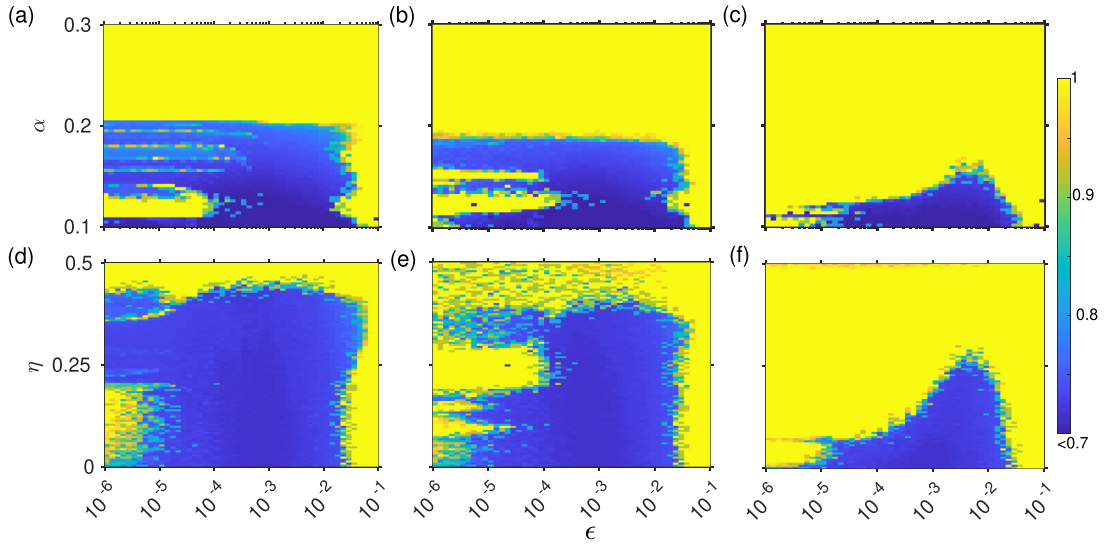


FIG. 7. Extent of synchronicity between the nodes as determined by the synchrony order parameter $\rho$. Shown for (a) and (d) $\gamma = 0$ (no frequency modulation), (b) and (e) $\gamma = 0.1$, and (c) and (f) $\gamma = 0.4$ is the synchrony measure in (a)–(c) the $(\epsilon, \alpha)$ plane for a fixed value of $\eta = 0.25$ and (d)–(f) the $(\epsilon, \eta)$ plane for a fixed value of $\alpha = 0.15$. The color bar corresponds to the value of synchrony order parameter $\rho$ in the interval (0.7,1). In both (a)–(c) and (d)–(f), the region of synchronicity increases with an increase in $\gamma$. The other parameter values are $\phi = 2$, $\mu = 1$, $w_0 = 0.541$, $w_f = 0.01$, $k = 1$, $p = 0$, and $N = 11$.

numerically obtained MLE. Nevertheless, from our simulation results, it is still apparent that with an increase in the strength of frequency modulation, the Arnold tongue region increases.

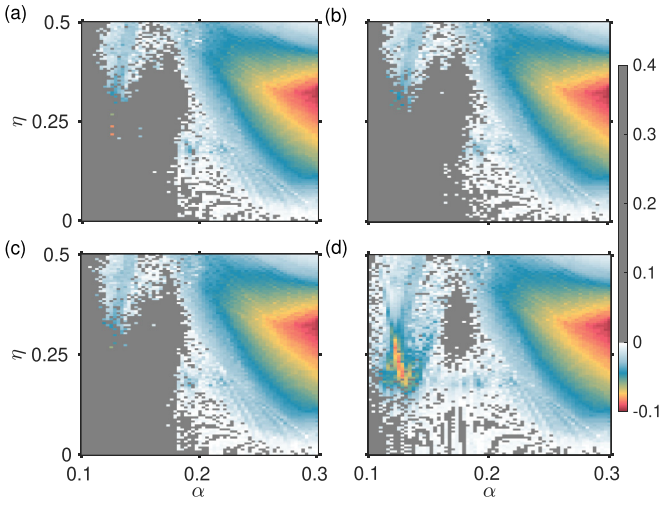


FIG. 8. Maximal Lyapunov exponent evaluated in the $(\alpha, \eta)$ parameter space of the spatial ecological network with frequency modulation $\gamma = 0.1$ and for variation in the rewiring probability $p$ and the average degree $k$. When $k = 2$, the MLE is obtained for different rewiring probabilities: (a) $p = 0$, representing a regular network, and (b) $p = 0.8$, for a small-world network. When $p = 0.2$, the MLE is obtained for different average degrees: (c) $k = 2$ and (d) $k = 5$. The color bar represents the MLE. The variation in $p$ has almost no effect. However, the variation in $k$ has a negligible effect on the stability as determined by negative values of the MLE. The other parameter values are $\phi = 2$, $\mu = 1$, $w_0 = 0.541$, $w_f = 0.01$, $\epsilon = 2^{-7}$, and $N = 21$.

Hence, it signifies that increasing time variability in the system induces synchronicity.

We also checked the generality of our results by studying a driven spatial ecological network where the nodes are connected following the small-world network topology [39]. For the spatial ecological network model, we found that in the weak-coupling limit (i.e., weak species dispersal strength), frequency modulation can induce synchrony and intermittent synchrony that is otherwise asynchronous. Further, we reduced the system to a phase equation to distinguish between synchrony, intermittent synchrony, and asynchrony. Then the numerically obtained phase differences differentiate the collective dynamics of the driven network. We also calculated a network synchrony order parameter showing that the degree of synchrony increases with increasing strength of frequency modulation. Focusing on the stable synchronous solution, we found that the rewiring probability has a negligible effect on the stability, as indicated by the MLE.

Overall, our study signifies that the time-dependent frequency of seasonal forcing can alter the synchronization pattern in ecosystems. Specifically, an increase in the time dependence of driving frequency increases the chance of population synchronization. This is fundamentally important for ecosystem management as synchrony in species dynamics creates interdependence in their abundance and concurrent low abundance can lead to concurrent extinction. Here we consider an ecosystem that exhibits periodic dynamics, and in the future, it would be interesting to know the dynamics of chaotic ecosystems under frequency modulation. Further, the role of oscillation amplitude on complex model dynamics needs to be uncovered. In the Kuramoto model, a discontinuous or first-order phase transition (also termed explosive synchronization) from incoherence to synchronization has been studied. In our model, we found that incoherence to

synchrony occurs via intermittent synchronization. However, it will certainly be interesting to investigate whether frequency modulation can trigger sudden synchronization transition in our network model.


## ACKNOWLEDGMENTS

P.S.D. acknowledges financial support from the Science and Engineering Research Board, Government of India (Grant No. MTR/2021/000148). S.B. acknowledges Dhruv Mittal for helpful discussion.


## APPENDIX: EFFECT OF THE STRENGTH OF FREQUENCY MODULATION ON THE REDUCED PHASE EQUATION

For different $\gamma$ (strength of the frequency modulation), we calculate the difference $x_i - x_1$ in the abundance of each node $x_i$ to that of the first oscillator $x_1$ of the network (3) [see Figs. 9(a) and 9(b)]. We also plot the phase difference $\theta_i - \theta_1$ of each reduced phase oscillator $\theta_i$ to the first oscillator $\theta_1$ [see Figs. 9(c) and 9(d)]. The network model and the corresponding phase-reduced model show similar results; with an increase in $\gamma$, the asynchronous dynamics turns into synchronous dynamics.

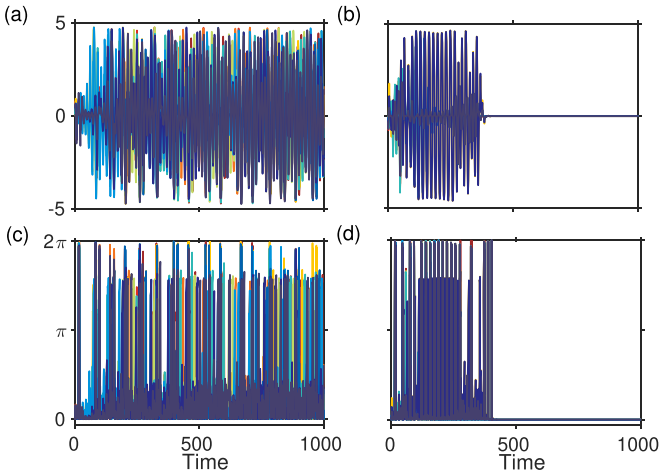


FIG. 9. Averaged differences in (a) and (b) species abundance $x_i - x_1$ and (c) and (d) phase $\theta_i - \theta_1$, depicting (a) and (c) asynchronous ($\gamma = 0$) and (b) and (d) synchronous dynamics ($\gamma = 0.4$), calculated for (a) and (b) the network model and (c) and (d) the corresponding phase-reduced model, by employing 100 randomly chosen initial conditions. The other parameter values are $\phi = 2$, $\alpha = 0.3$, $\mu = 1$, $\eta = 0.25$, $w_0 = 0.541$, $w_f = 0.01$, $\epsilon = 2^{-7}$, $k = 1$, $p = 0$, and $N = 11$.


[1] R. M. May, Science **177**, 900 (1972).
[2] B. E. Kendall, C. J. Briggs, W. W. Murdoch, P. Turchin, S. P. Ellner, E. McCauley, R. M. Nisbet, and S. N. Wood, Ecology **80**, 1789 (1999).
[3] A. Hastings and T. Powell, Ecology **72**, 896 (1991).
[4] B. Blasius, A. Huppert, and L. Stone, Nature (London) **399**, 354 (1999).
[5] F. Barraquand, S. Louca, K. C. Abbott, C. A. Cobbold, F. Cordoleani, D. L. DeAngelis, B. D. Elderd, J. W. Fox, P. Greenwood, F. M. Hilker *et al.*, Ecol. Lett. **20**, 1074 (2017).
[6] J. Vandermeer, BioScience **56**, 967 (2006).
[7] A. Gupta, T. Banerjee, and P. S. Dutta, Phys. Rev. E **96**, 042202 (2017).
[8] J. Huisman and F. J. Weissing, Nature (London) **402**, 407 (1999).
[9] S. Rinaldi, S. Muratori, and Y. Kuznetsov, Bull. Math. Biol. **55**, 15 (1993).
[10] B. Blasius, L. Rudolf, G. Weithoff, U. Gaedke, and G. F. Fussmann, Nature (London) **577**, 226 (2020).
[11] O. N. Bjørnstad, W. Falck, and N. C. Stenseth, Proc. R. Soc. B **262**, 127 (1995).
[12] R. A. Taylor, A. White, and J. A. Sherratt, Proc. R. Soc. B **280**, 20122714 (2013).
[13] M. Pascual and S. P. Ellner, Ecology **81**, 2767 (2000).
[14] M. Lucas, J. Newman, and A. Stefanovska, Phys. Rev. E **97**, 042209 (2018).
[15] M. Lucas, D. Fanelli, and A. Stefanovska, Phys. Rev. E **99**, 012309 (2019).
[16] T. M. Massie, B. Blasius, G. Weithoff, U. Gaedke, and G. F. Fussmann, Proc. Natl. Acad. Sci. USA **107**, 4236 (2010).
[17] R. Arumugam and P. S. Dutta, Phys. Rev. E **97**, 062217 (2018).
[18] C. Zhou and J. Kurths, Phys. Rev. Lett. **88**, 230602 (2002).
[19] A. Pikovsky, M. Rosenblum, and J. Kurths, *Synchronization: A Universal Concept in Nonlinear Science* (Cambridge University Press, Cambridge, 2003).
[20] K. C. Abbott, Ecol. Lett. **14**, 1158 (2011).
[21] S. Ahn and L. L. Rubchinsky, J. Theor. Biol. **490**, 110159 (2020).
[22] H. Fan, L.-W. Kong, X. Wang, A. Hastings, and Y.-C. Lai, Natl. Sci. Rev. **8**, nwaa269 (2021).
[23] Z. Hagos, T. Stankovski, J. Newman, T. Pereira, P. V. McClintock, and A. Stefanovska, Philos. Trans. R. Soc. A **377**, 20190275 (2019).
[24] A. Hastings, K. C. Abbott, K. Cuddington, T. B. Francis, Y.-C. Lai, A. Morozov, S. Petrovskii, and M. L. Zeeman, J. R. Soc. Interface **18**, 20210257 (2021).
[25] M. L. Rosenzweig and R. H. MacArthur, Am. Nat. **97**, 209 (1963).
[26] M. D. Holland and A. Hastings, Nature (London) **456**, 792 (2008).
[27] V. Dakos, E. Benincà, E. H. van Nes, C. J. Philippart, M. Scheffer, and J. Huisman, Proc. R. Soc. B **276**, 2871 (2009).
[28] S. Bhandary, T. Kaur, T. Banerjee, and P. S. Dutta, Phys. Rev. E **103**, 022314 (2021).
[29] R. M. Smeal, G. B. Ermentrout, and J. A. White, Philos. Trans. R. Soc. B **365**, 2407 (2010).
[30] W. Kurebayashi, S. Shirasaka, and H. Nakao, Phys. Rev. Lett. **111**, 214101 (2013).
[31] E. E. Goldwyn and A. Hastings, Theor. Popul. Biol. **73**, 395 (2008).
[32] E. E. Goldwyn and A. Hastings, Bull. Math. Biol. **71**, 130 (2009).

[33] G. B. Ermentrout, J. Math. Biol. **12**, 327 (1981).

[34] Y. Kuramoto, *Chemical Oscillations, Waves, and Turbulence*, Springer Series in Synergetics Vol. 19 (Springer, Berlin, Heidelberg, 1984), Chap. 7, pp. 111–140.

[35] G. B. Ermentrout and D. H. Terman, in *Mathematical Foundations of Neuroscience*, edited by S. S. Antman, J. E. Marsden, L. Sirovich, and S. Wiggins, Interdisciplinary Applied Mathematics Vol. 35 (Springer, New York, 2010).

[36] I. G. Malkin, *Some Problems in the Theory of Nonlinear Oscillations* (U.S. Atomic Energy Commission, Washington, DC, 1959), Vol. 1.

[37] N. Komin, A. C. Murza, E. Hernández-García, and R. Toral, Interface Focus **1**, 167 (2011).

[38] N. Stollenwerk, P. F. Sommer, B. Kooi, L. Mateus, P. Ghaffari, and M. Aguiar, Ecol. Complex. **30**, 91 (2017).

[39] E. Ranta, M. S. Fowler, and V. Kaitala, Proc. R. Soc. B **275**, 435 (2008).